

Rainfall Advection using Velocimetry by Multiresolution Viscous Alignment *

Sai Ravela

Earth, Atmospheric and Planetary Sciences

Virat Chatdarong

Civil and Environmental Engineering

Massachusetts Institute of Technology

ravela@mit.edu

April 10, 2006

Abstract

An algorithm to estimate motion from satellite imagery is presented. Dense displacement fields are computed from time-separated images of significant convective activity using a Bayesian formulation of the motion estimation problem. Ordinarily this motion estimation problem is ill-posed; there are far too many degrees of freedom than necessary to represent the motion. Therefore, some form of regularization becomes necessary and by imposing smoothness and non-divergence as desirable properties of the estimated displacement vector field, excellent solutions are obtained. Our approach provides a marked improvement over other methods in conventional

*This material is supported in part by NSF ITR 0121182 and DDDAS 0540259.

use. In contrast to correlation based approaches, the displacement fields produced by our method are dense, spatial consistency of the displacement vector field is implicit, and higher-order and small-scale deformations can be easily handled. In contrast with optic-flow algorithms, we can produce solutions at large separations of mesoscale features between large time-steps or where the deformation is rapidly evolving.

1 Introduction

Environmental data assimilation is the methodology for combining imperfect model predictions with uncertain data in a way that acknowledges their respective uncertainties. The proper framework for state estimation includes sequential [15], ensemble-based [14] and variational [20, 5] methods.

The difficulties created by improperly represented error are particularly apparent in mesoscale meteorological phenomena such as thunderstorms, squall-lines, hurricanes, precipitation, and fronts. We are particularly interested in rainfall data-assimilation, where rainfall measurements from satellite data, radar data, or in-situ measurements are used to condition a rainfall model. Such conditional simulations are valuable both for producing estimates at the current time (nowcasting), as well as for short-term forecasting.

There are a countless number of models developed to simulate the rainfall process. In general, there are two types of models that can deal with spatial and

temporal characteristics of rainfall. The first category is the meteorological model or the quantitative precipitation forecasting model. It involves a large, complex set of differential equations seeking to represent complete physical processes controlling rainfall and other weather related variables. Examples of these models include the fifth-generation Mesoscale Model (MM5) [3, 4, 16], the step-mountain Eta coordinate model [1, 2, 13], and the Regional Atmospheric Modeling System (RAMS) [7, 12], etc. The second type is the spatiotemporal stochastic rainfall model. It aims to summarize the spatial and temporal characteristics of rainfall by a small set of parameters [6, 18, 11, 8, 22, 25]. This type of model usually simulates the birth and decay of rain-cells and evolve them through space and time using simple physical descriptions. Despite significant differences among these rainfall models, the concept of propagating rainfall through space and time are relatively similar.

The major ingredient required to advect rainfall is a velocity field. Large spatial-scale (synoptic) winds are inappropriate for this purpose for a variety of reasons. Ironically, synoptic observations can be sparse to be used directly and although synoptic-scale wind analyses produced from them (and models) do produce dense spatial estimates, such estimates often do not contain variability at the meso-scales of interest. The motion of mesoscale convective activity is a natural source for velocimetry. Indeed, there exist products that deduce “winds” by estimating the motion of temperature, vapor and other fields evolving in time [9, 10].

In this paper, we present an algorithm for velocimetry from observed motion from satellite observations such as GOES, AMSU, TRMM, or radar data such as NOWRAD. This algorithm follows from a Bayesian formulation of the motion estimation problem, where a dense displacement field is estimated from two images of cloud-top temperature of rain-cells separated in time. Ordinarily, the motion estimation problem is ill-posed, because the displacement field has far too many degrees of freedom than the motion. Therefore, some form of regularization becomes necessary and by imposing smoothness and non-divergence as desirable properties of the estimated displacement vector field solutions can be obtained.

This approach provides marked improvement over other methods in conventional use. In contrast to correlation based approaches used for deriving velocity from GOES imagery, the displacement fields are dense, quality control is implicit, and higher-order and small-scale deformations can be easily handled. In contrast with optic-flow algorithms [21, 17], we can produce solutions at large separations of mesoscale features between large time-steps or where the deformation is rapidly evolving.

After formulating the motion estimation problem and providing a solution, we extend the algorithm using a multi-resolution procedure. The primary advantage of a multi-resolution approach is to produce displacement fields quickly. The secondary advantage is to structure the estimation homotopically; coarse or low-frequency information is used first to produce velocity estimates over which

deformation adjustments from finer-scale structures is superposed. The result is a powerful algorithm for velocimetry by alignment. As such, it is useful in a variety of situations including, for example, (a) estimating winds, (b) estimating transport of tracers, (c) Particle Image Velocimetry, (d) Advecting Rainfall models etc.

2 Related Work

There are two dominant approaches to computing flow from observations directly. The first is correlation-based and the second is based on optic flow.

In correlation based approaches [19], a region of interest (or patch) is identified in the first image and correlated within a search window in the second image. The location of the best match is then used to compute a displacement vector. When the input image or field is tiled, possibly overlapping, and regions of interest are extracted from each tile location, the result is velocimetry at regular intervals and is most commonly used for Particle Image Velocimetry (PIV). In certain instances it is useful to define interest-points or salient features around which to extract regions of interest. In particular, if the field has many areas with negligible spatial variability, then matches are undefined. As a quality control measure then, matching is restricted only to those regions of interest that have interesting variability, or interest points.

There are several disadvantages to correlation-based approaches. First, by

construction it is assumed that the entire ROI purely translates from one image to the other. This is not always the case, but is a reasonable approximation when the right length scale can be found. However, when higher-order deformations (shears for example) are present, correlation based approaches cannot be expected to work well. Second, correlation based approaches assume that a unique match can be found in a way that is substantially better than correlation elsewhere. This is only true if the features are well-defined and identified. Third, there is no implicit consistency across regions of interest in correlation-based flow. Neighboring regions of interest can and often do match at wildly different and inconsistent locations. This calls for a significant overhead in terms of quality control. Fourth, it is not clear how the search window size (that is the area over which a region of interest is matched in the subsequent frame) is determined. This window size varies both in space (as the velocity varies spatially) and time (as velocity varies with time). A larger search window portends a larger probability to miss the real target, and a smaller search window can lead to false negatives or false positives. Finally, where interest points are used as a preprocessing step to correlation, the velocity field produced is necessarily sparse, and therefore, leaves hanging the question of how to produce dense flow fields. Our proposed algorithm handles all these issues in a simple and direct way.

More closely related to the proposed approach is optic flow [21, 17]. This method arises from what is known as the brightness constraint equation, which

is a statement of conservation of brightness (intensity) mass, expressed by the continuity equation evaluated at each pixel or grid node of X .

$$\frac{\partial X}{\partial t} + \mathbf{q} \cdot \nabla X = 0 \quad (1)$$

Here X is the brightness or intensity scalar field and \mathbf{q} a displacement vector-field. Solutions to the optic flow equation can be formulated using the well-known method by [21], which can be stated as a solution to the following system of equations:

$$(\nabla X)(\nabla X)^T \mathbf{q} = -(\nabla X) \frac{\partial X}{\partial t} \quad (2)$$

The right-hand side is completely determined from a pair of images and the coefficient or stiffness matrix on the left-hand side is the second-derivative of the auto correlation matrix, also known as the windowed second-moment matrix, or Harris interest operator, which is sensitive to “corners” in an image. This formulation arises directly from a quadratic formulation, which can in turn be synthesized from a Bayesian formulation under a Gaussian assumption. Thus, we can write that we seek to minimize

$$J(\mathbf{q}) = ||X(\mathbf{r} - \mathbf{q}) - Y|| \quad (3)$$

Then solve this problem via the Euler-Lagrange equation:

$$\frac{\partial J(\mathbf{q})}{\partial \mathbf{q}} = \nabla X|_{\mathbf{r}-\mathbf{q}}(X(\mathbf{r}-\mathbf{q}) - Y) = 0 \quad (4)$$

The solution is obtained by *linearizing* (4), that is,

$$\begin{aligned} \nabla X|_{\mathbf{r}-\mathbf{q}}(X(\mathbf{r}) - \nabla X \cdot \mathbf{q} - Y) &= 0 \\ \nabla X(\nabla X)^T \mathbf{q} &= -\nabla X(Y - (X(\mathbf{r}))) \end{aligned} \quad (5)$$

There are several disadvantages to this algorithm. First, much like correlation with feature detection, equation 5 is evaluated at pixels where the second-moment matrix is full-rank, which corresponds to locations where features are present. There is no clear way of propagating information obtained at sparse locations to locations where direct computation of displacement is not possible due to poor conditioning of the second-moment matrix. For the same reason, it cannot handle tangential flows. The brightness constraint equation can only represent flows along brightness streamlines. When tangential motion is present, detected motion at extreme ends a moving curve cannot be propagated easily into the interior. Our method provides some degree of spatial smoothness common in geophysical fluid transport, and uses regularization constraints to propagate flow information to nodes where feature strengths are weak.

Second, the linearization implicit in (5) precludes large displacements; structures must be closely overlapping in successive images, which can also be seen

from the continuity equation (1). Therefore, this method is very useful for densely sampled motion, such as ego-motion resulting from a moving, jittering camera, but is not as useful for sparsely sampled flow arising from structures moving in a scene. In the latter case, to ameliorate the effects of large expected displacement, multi-resolution approaches have been proposed. Even so, much like determining the size of the search window in correlation, determining the number of resolutions is an ad-hoc procedure. Our method can handle large displacements and we also propose a multi-resolution approach, but the primary motivation there is improved computational speed.

3 Velocimetry by Field Alignment

The main approach consists of solving a nonlinear quadratic estimation problem for a field of displacements. Solutions to this problem are obtained by regularizing the an ill-posed inverse problem. The material presented in this section is derived directly from work by Ravela [24], and Ravela et al. [23]. Here we reformulate their original formulation to allow only position adjustments.

To make this framework more explicit it is useful to introduce some notation. Let $X = X(\mathbf{r}) = \{X[\underline{r}_1^T] \dots X[\underline{r}_m^T]\}$ be the first image, written as a vector, defined over a spatially discretized computational grid Ω , and $\mathbf{r}^T = \{\underline{r}_i = (x_i, y_i)^T, i \in \Omega\}$ be the position indices. Let \mathbf{q} be a *vector* of displacements, that

is $\mathbf{q}^T = \{\underline{q}_i = (\Delta x_i, \Delta y_i)^T, i \in \Omega\}$. Then the notation $X(\mathbf{r} - \mathbf{q})$ represents *displacement* of X by \mathbf{q} . The displacement field \mathbf{q} is real-valued, so $X(\mathbf{r} - \mathbf{q})$ must be evaluated by interpolation if necessary. It is important to understand that this displacement field represents a warping of the underlying grid, whose effect is to move structures in the image around, see Figure 1.

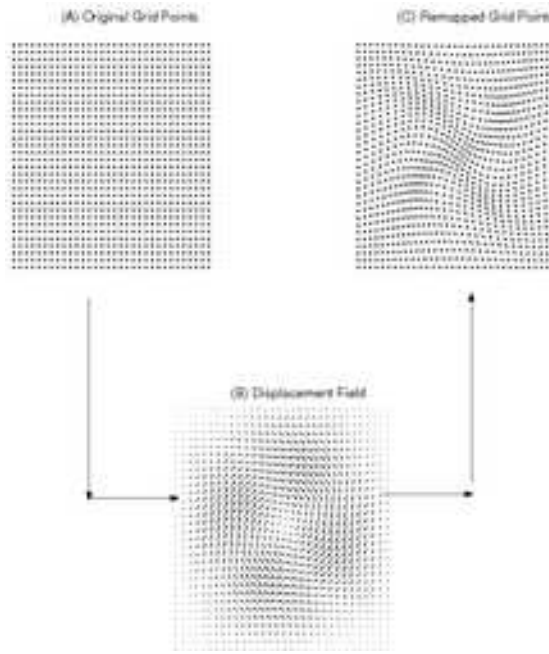


Figure 1: A graphical illustration of field alignment. State vector on a discretized grid is moved by deforming its grid (\mathbf{r}) by a displacement (\mathbf{q}).

In a probabilistic sense, we may suppose that finding \mathbf{q} that has the maximum a posteriori probability in the distribution $P(\mathbf{q}|\mathcal{X}, \mathcal{Y})$ is appropriate. Without loss of generality, \mathcal{X} is a random variable corresponding to the image or field at a given time and \mathcal{Y} is random variable for a field at a future time. Using Bayes rule we

obtain $P(Q = \mathbf{q} | \mathcal{X} = X, \mathcal{Y} = Y) \propto P(\mathcal{Y} = Y, \mathcal{X} = X | \mathbf{q})P(\mathbf{q})$. If we make a Gaussian assumption of the component densities, we can write:

$$P(X, Y | \mathbf{q}) = \frac{1}{(2\pi)^{\frac{n}{2}} |R|^{\frac{1}{2}}} e^{-\frac{1}{2}(Y - X(\mathbf{r} - \mathbf{q}))^T R^{-1} (Y - X(\mathbf{r} - \mathbf{q}))} \quad (6)$$

This equation says that the observations separated in time can be related using a Gaussian model to the displaced state $X(\mathbf{r} - \mathbf{q})$, where $X(\mathbf{r})$ is defined on the original grid, and \mathbf{q} is a displacement field. We use the linear observation model here, and therefore, $Y = HX(\mathbf{r} - \mathbf{q}) + \eta, \eta \sim N(0, R)$. We should emphasize here that the observation vector is fixed. It's elements are always defined from the original grid. In fully observed fields, H is an identity matrix, and for many applications R , reflecting the noise in the field, can also be modeled as an identity matrix.

$$P(\mathbf{q}) = \frac{1}{C} e^{-L(\mathbf{q})} \quad (7)$$

This equation specifies a *displacement prior*. This prior is constructed from an energy function $L(\mathbf{q})$ which expresses constraints on the displacement field. The proposed method for constructing L is drawn from the nature of the expected displacement field. Displacements can be represented as smooth flow fields in many fluid flows and smoothness naturally leads to a Tikhonov type formulation

[26] and, in particular, $L(\mathbf{q})$ is designed as a gradient and a divergence penalty term. These constraints, expressed in quadratic form are:

$$L(\mathbf{q}) = \frac{w_1}{2} \sum_{j \in \Omega} \text{tr}\{[\nabla \underline{q}_j][\nabla \underline{q}_j]^T\} + \frac{w_2}{2} \sum_{j \in \Omega} [\nabla \cdot \underline{q}_j]^2 \quad (8)$$

In Equation 8, \mathbf{q}_j refers to the j^{th} grid index and tr is the trace. Equation 8 is a *weak constraint*, weighted by the corresponding weights w_1 and w_2 . Note that the constant C can be defined to make Equation 7 a proper probability density. In particular, define $Z(\mathbf{q}) = e^{-L(\mathbf{q})}$ and define $C = \int_{\mathbf{q}} Z(\mathbf{q}) d\mathbf{q}$. This integral exists and converges.

With these definitions of probabilities, we are in a position to construct an objective by evaluating the log probability. We propose a solution using Euler-Lagrange equations. Defining $\mathbf{p} = \mathbf{r} - \mathbf{q}$ These can be written as:

$$\frac{\partial J}{\partial \mathbf{q}} = \nabla X|_{\mathbf{p}} H^T R^{-1} (H X(\mathbf{p}) - Y) + \frac{\partial L}{\partial \mathbf{q}} = 0 \quad (9)$$

Using the regularization constraints (9) at a node i now becomes:

$$w_1 \nabla^2 \underline{q}_i + w_2 \nabla(\nabla \cdot \underline{q}_i) + \left[\nabla X^f|_{\mathbf{p}} H^T R^{-1} (H [X^f(\mathbf{p})] - Y) \right]_i = 0 \quad (10)$$

Equation 10 is the field alignment formulation. It introduces a forcing based on the residual between the model- and observation-fields. The constraints on the

displacement field allow the forcing to propagate to a consistent solution. Equation 10 is also non-linear, and is solved iteratively, as a Poisson equation. During each iteration \mathbf{q} is computed by holding the forcing term constant. The estimate of displacement at each iteration is then used to deform a copy of the original forecast model-field using bi-cubic interpolation for the next iteration. The process is repeated until a small displacement residual is obtained, the misfit with observations does not improve, or an iteration limit is reached. Upon convergence, we have an aligned image $X(\hat{\mathbf{p}})$, and a displacement field $\hat{\mathbf{q}} = \sum_{d=1}^N q^{(d)}$, for individual displacements $q^{(d)}$ at iterations $d = 1 \dots D$

3.1 Multi-resolution Alignment and Velocimetry

The convergence of solution to the alignment equation is super-linearly dependent on the expected displacement between the two fields. Therefore, it is desirable to solve it in a coarse-to-fine manner, which serves two principal advantages. The first, as the following construction will show, is to substantially speed-up the time to alignment because decimated (or coarse-resolution) representations of a pair of fields has smaller expected displacement than a pair at finer resolution.

Second, decimation or resolution reduction also implies that finer structure or higher spatial frequencies will be attenuated. This smoothness in the coarsened-field intensities directly translates to smoothness in flow-fields using (9). Thus, a

coarse-to-fine method for alignment can incrementally add velocity contributions from higher-frequencies, that is it incrementally incorporates higher-order variability in the displacement field. Many of the advantages of a multi-resolution approach have been previously explored in the context of visual motion estimation, including the famous pyramid algorithm and architecture for matching and flow and our implementation borrows from this central idea.

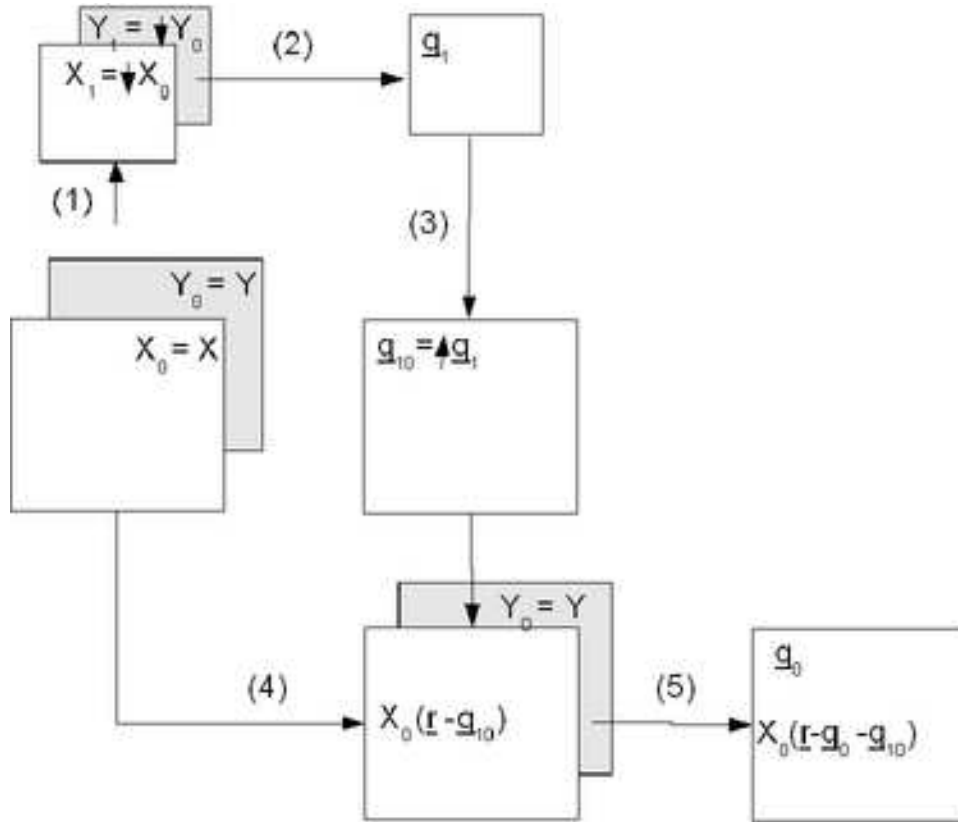


Figure 2: The multi-resolution algorithm is shown for two-levels and requires five steps, labeled (1) through (5). See text for explanation.

The multi-resolution algorithm is depicted in Figure 2 for two levels. The

input images X and Y are decimated to generate coarse resolution images X_1 and Y_1 respectively (step 1). Let us suppose that this scaling is by a factor of $0 < s < 1$ (most commonly $s = 0.5$). Displacement is computed for this level first, and let us call this $\hat{\mathbf{q}}_1$ (step 2). This displacement field is downsampled by a factor of s , using simple (bicubic) interpolation, to produce a prior estimate of displacement at level 0, written $\hat{\mathbf{q}}_{10} = s^{-1}\hat{\mathbf{q}}_0(s^{-1}\mathbf{r})$ (step 3). The source image at level 0, that is $X_0 = X$ is displaced by $\hat{\mathbf{q}}_{10}$ (step 4) and thus $X(\mathbf{r} - \hat{\mathbf{q}}_{10})$ is aligned with Y_0 to produce a displacement estimate $\hat{\mathbf{q}}_0$ (step 5). The total displacement relating source image X with target field Y is simply $\hat{\mathbf{q}}_0 + \hat{\mathbf{q}}_{10}$. Multiple levels of resolution can be implemented from this framework recursively.

4 Example

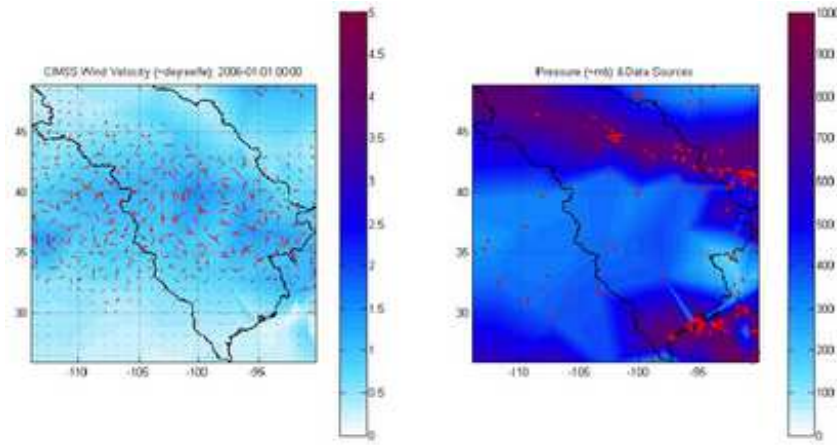


Figure 3: CIMSS Winds derived from GOES data at 2006-04-06-06Z (left) and pressure (right). The velocity vectors are sparse and contain significant divergence.

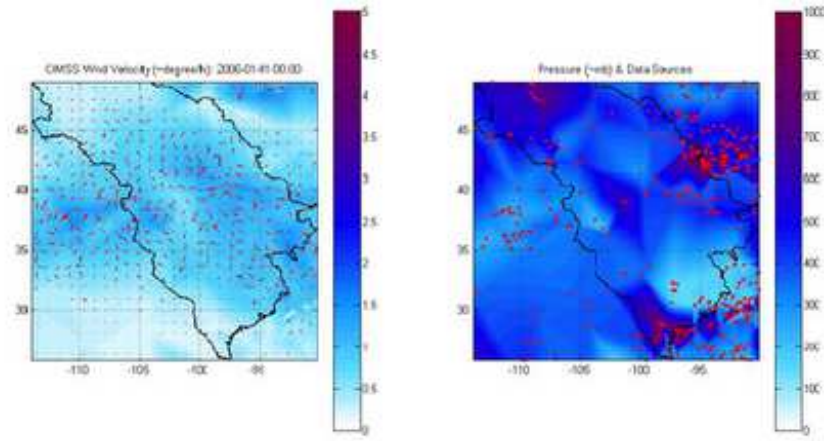


Figure 4: CIMSS Winds derived from GOES data at 2006-04-06-09Z (left) and pressure (right). The velocity vectors are sparse and contain significant divergence.

The performance of this algorithm is illustrated in a velocimetry computation. To compare, we use CIMSS wind-data satellite data [10], depicted in Figure 3, and Figure 4 obtained from CIMSS analysis on 2006-06-04 at 06Z and 09Z respectively. CIMSS wind-data is shown over the US great plains, and were obtained from the 'sounder.' The red dots indicate the original location of the data. The left subplot shows wind speed (in degree/hr). The right ones show pressure, and the location of raw measurements in red.

It can be seen in the maps shown in Figure 3 and Figure 4 that current method to produce winds generate sparse vectors and, further, has substantial divergence. Whilst this can be thought of as accurately representing turbulence, in reality these vectors are more likely the result of weak quality control. The primary methodology used here is to identify features in an image, extract regions of interest around

them and search for them in subsequent frames. This, by definition produces sparse velocity estimates (features are sparse), leaving unanswered how to systematically incorporate appropriate spatial interpolation functions for the velocity. Since regions of interest are essentially treated as being statistically independent, mismatches can produce widely varying displacement vectors. Such mismatches can easily occur in correlation based approaches when the features are not distinguishing or substantial deformations occur from one time to another in a region of interest. A more detailed discussion is presented in Section 2.

In contrast, our method produces dense flow fields, and quality control is implicit from regularization constraints. Figure 5(a,b) shows a pair of NOWRAD images at 2006-06-01-0800Z and 2006-06-01-0900Z respectively, and the computed flow field in Figure 5(c). Similarly, Figure 5(d,e,f) show the GOES images and velocity from the same time frame over the deep convective rainfall region in the Great Plains example. The velocities are in good agreement with CIMSS derived winds where magnitudes are concerned, but the flow-fields are smooth and visual confirmation of the alignment provides convincing evidence that they are correct.

5 Conclusions

Our method is a Bayesian perspective of the velocimetry problem. It has several distinct advantages: (a) It is useful for a wide range of observation modalities. (b) Our approach does not require features to be identified for computing velocity. This is a significant advantage because features cannot often be clearly delineated, and are by definition sparse. (c) Our approach implicitly uses quality control in terms of smoothness, and produces dense flow-fields. (d) our approach can be integrated easily with current operational implementations, thereby making this effort more likely to have a real impact. Finally, it should be noted that the regularization constraint in field alignment is a weak constraint and the weights determine how strongly the constraints influence the flow field. The constraint in L is modeled as such because we expect the fluid flow to be smooth. From a regularization point of view, there can be other choices [27] as well. The proposed method can be used for a variety of velocimetry applications including PIV, velocity from tracer-transport, and velocity from GOES and other satellite data, and an application of this is to advect rain-cells produced by a rainfall model, with realistic wind-forcing.

References

- [1] T. L. Black. The new nmc moesoscale eta model: Description and forecast examples. *Weather and Forecasting*, 9(2):265–278, 1994.
- [2] T. L. Black, D. Deaven, and G. DiMego. The step-mountain eta coordinate model: 80 km early version and objective verifications. *NWS/NOAA Tech. Procedures Bull.*, 1993. 412: p. 31., 412:31, 1993.
- [3] F. Chen and J. Dudhia. Coupling an advanced land surface-hydrology model with the penn state-ncar mm5 modeling system. part i: Model implementation and sensitivity. *Monthly Weather Review*, 129(4):569–585, 2001.
- [4] F. Chen and J. Dudhia. Coupling an advanced land surface-hydrology model with the penn state-ncar mm5 modeling system. part ii: Preliminary model validation. *Monthly Weather Review*, 129(4):587–604, 2001.
- [5] P. Courtier. Variational methods. *J. Meteor. Soc. Japan*, 75, 1997.
- [6] P. Cowpertwait. Further developments of the neyman-scott clustered point process for modeling rainfall. *Water Resource Research*, 27(7), 1991.
- [7] A. Orlandi et al. Rainfall assimilation in rams by means of the kuo parameterisation inversion: Method and preliminary results. *Journal of Hydrology*, 288(1-2):20–35, 2004.

- [8] C. Onof et al. Rainfall modelling using poisson-cluster processes: A review of developments. *Stochastic Environmental Research and Risk Assessment*, 2000.
- [9] C. S. Velden et al. Upper-tropospheric winds derived from geostationary satellite water vapor observations. *Bulletin of the American Meteorological Society*, 78(2):173–195, 1997.
- [10] C. Velden et al. Recent innovations in deriving tropospheric winds from meteorological satellites. *Bulletin of the American Meteorological Society*, 86(2):205–223, 2005.
- [11] H. Moradkhani et al. Dual state-parameter estimation of hydrological models using ensemble kalman filter. *Advances in Water Resources*, 28(2):135–147, 2005.
- [12] R. A. Pielke et al. A comprehensive meteorological modeling system rams. *Meteorology and Atmospheric Physics*, 49(1-4):69–91, 1992.
- [13] R. Rogers et al. Changes to the operational ”early” eta analysis forecast system at the national centers for environmental prediction. *Weather and Forecasting*, 11(3):391–413, 1996.
- [14] G. Evensen. The ensemble kalman filter: Theoretical formulation and practical implementation. *Ocean Dynamics*, 53:342–367, 2003.

- [15] A. Gelb. *Applied Optimal Estimation*. MIT Press, 1974.
- [16] G. Grell, J. Dudhia, and D.R. Stauffer. A description of the fifth generation penn state/ncar mesoscale model (mm5). Technical Report TN-398+IA, NCAR, 1993.
- [17] D. J. Heeger. Optical flow from spatiotemporal filters. *International Journal of Computer Vision*, pages 279–302, 1988.
- [18] M. N. Khaliq and C. Cunnane. Modelling point rainfall occurrences with the modified bartlett-lewis rectangular pulses model. *Journal of Hydrology*, 180(1):109–138, 1996.
- [19] D. T. Lawton. Processing translational motion sequences. *Computer Vision, Graphics and Image Processing*, 22:116–144, 1983.
- [20] A. C. Lorenc. Analysis method for numerical weather predictin. *Q. J. R. Meteorol. Soc.*, 112:1177–1194, 1986.
- [21] H.-H Nagel. Displacement vectors derived from second order intensity variations in image sequences. *Computer Vision, Graphics and Image Processing*, 21:85–117, 1983.

- [22] T. M. Over and V. K. Gupta. A space-time theory of mesoscale rainfall using random cascades. *Journal of Geophysical Research*, 101(D21):319–332, 1996.
- [23] S. Ravela. Amplitude-position formulation of data assimilation. In *ICCS 2006, Lecture Notes in Computer Science*, number 3993 in Part III, pages 497–505, 2006.
- [24] S. Ravela, K. Emanuel, and D. McLaughlin. Data assimilation by field alignment. *Physica (D)* - to appear, 2006.
- [25] I. Rodriguez-Iturbe, D.R. Cox, and V. Isham. A point process model for rainfall: Further developments. *Proceedings of the Royal Society of London. Series A, Mathematical and Physical Sciences*, 417(1853):283–298, 1988.
- [26] A.N. Tikhonov and V. Y. Arsenin. *Solutions of Ill-Posed Problems*. Wiley, New York, 1977.
- [27] G. Wabha and J. Wendelberger. Some new mathematical methods for variational objective analysis using splines and cross-validation. *Monthly Weather Review*, 108, 1980.

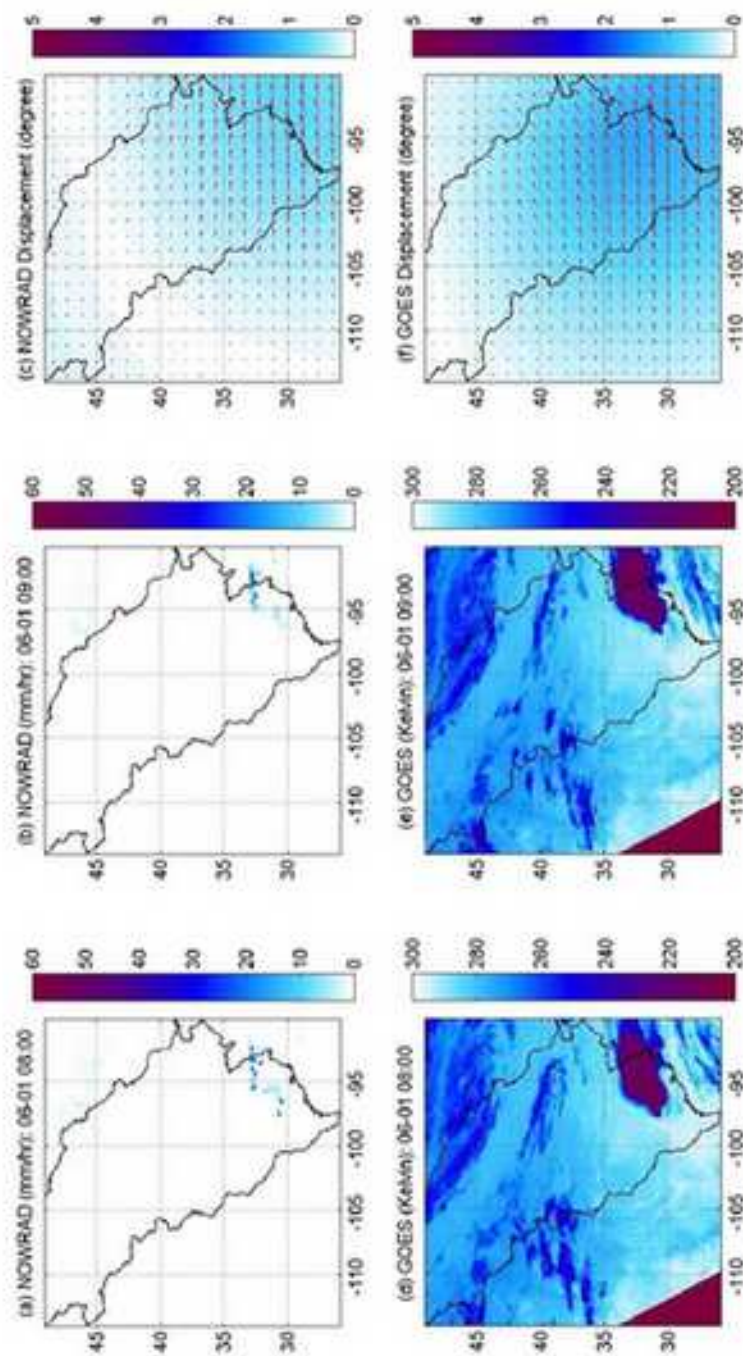


Figure 5: Deriving velocimetry information from satellite observations, Nexrad (top), GOES (bottom). See text for more information.